The International Journal of Advanced Manufacturing Technology
https://doi.org/10.1007/s00170-018-2137-0

ORIGINAL ARTICLE

Feedrate modulation for accurate traversal of trimmed planar offset paths

Rida T. Farouki[1] · **Jyothirmai Srinathu**[1]

Received: 1 March 2018 / Accepted: 7 May 2018
© Springer-Verlag London Ltd., part of Springer Nature 2018

Abstract

In milling planar shapes with cylindrical tools, CNC machines must employ tool paths offset from the desired part shape by the tool radius. To prevent gouging the part geometry and to ensure continuous paths, the offset path construction invokes *trimming* and *filling* operations at tangent discontinuities of the part shape, and smooth concave regions where the tool radius exceeds the part radius of curvature. A constant feedrate of the tool center along the offset path can result in large chip load variations. Conversely, a variable feedrate that (approximately) achieves a constant chip load can cause large acceleration/deceleration rates at the tool center. Moreover, feedrate reduction is required in the vicinity of the trimmed offset path tangent discontinuities, to ensure accurate execution and to minimize vibrations. A feedrate modulation methodology for trimmed offset paths is proposed, incorporating user-specified parameters to balance the competing demands of minimizing path contour error, chip load variations, and the overall traversal time. The feedrate modulation scheme is compatible with simple real-time interpolator algorithms, and its practical performance is demonstrated by real-time data obtained from several experiments performed on a CNC mill with an open-architecture software controller.

Keywords Tool radius compensation · Offset tool paths · Feedrate modulation · CNC machine · Real-time interpolator · Open-architecture controller

1 Introduction

Modern computer-aided design and manufacturing (CAD/CAM) technology has revolutionized the accuracy, efficiency, and consistency with which mass production of complex part shapes is possible. Since finite-size tools are used to cut parts, the tool center must follow paths offset from the desired part by displacements dependent on the tool size and geometry. These offset paths have—even in the case of a planar shape cut by a cylindrical tool—a much more complicated geometry than the desired part shape.

The *untrimmed offset* to any given piecewise–smooth closed planar curve C is the locus generated by the vector $d\,\mathbf{n}$, where the distance d is the tool radius and $\mathbf{n}$ is the unit normal vector (at points of tangent discontinuity, $\mathbf{n}$ executes a finite rotation defined by the angular extent of the discontinuity). The untrimmed offset has the property that each point is distance d from the corresponding point of C, but not necessarily distance d from *every* point of C. The locus with the latter property, which is the desired path for gouge-free machining by a tool of radius d, is the *trimmed offset* [17, 18].

The offset trimming process, which derives the trimmed offset from the untrimmed offset, is usually performed off-line due to its inherent complexity: it involves computing all self-intersection points of the untrimmed offset, and then identifying which segments delineated by these points are at distance d from the entire curve C. For simple (polygonal) curves, pre-computing the Voronoi diagram can facilitate the offset trimming procedure [23], but more sophisticated methods are required [15] to compute self-intersections of the offsets to free-form curves. For cases where these self-intersections arise only from "local" interference (concave tangent discontinuities or concave regions of high curvature)—e.g., finish-machining applications—an algorithm has been developed in [20] to perform *real-time* offset trimming by incorporating a point/curve distance function within the CNC interpolator.

✉ Rida T. Farouki
farouki@ucdavis.edu

Jyothirmai Srinathu
jsrinathu@ucdavis.edu

[1] Department of Mechanical and Aerospace Engineering, University of California, Davis, CA 95616, USA

Published online: 24 May 2018

The focus of the present study is not on the generation of trimmed offset paths, but rather on the modulation of feedrate along them in a manner that balances the competing requirements of contour error reduction, suppression of machining force variations, management of inertial forces associated with rapid tool acceleration/deceleration, and minimization of total traversal time.

Feedrate modulation in the execution of free-form tool paths has been an active topic of research in recent years, motivated by considerations such as satisfaction of axis acceleration or jerk constraints, the efficient execution of smoothed sharp corners, minimization of contour error, the identification of time-optimal motion solutions, etc.—see, for example [1, 2, 5–7, 9–11, 21, 24, 27, 28, 30, 31, 33, 38, 39, 42]. In these prior studies, the tool paths are usually assumed to be defined as spline curves—often NURBS (non-uniform rational B-splines). Although NURBS have been widely adopted as a CAD geometry standard, in finish-machining a shape specified by a NURBS curve (or rough-cutting using contour-parallel paths), the tool must execute *offset* paths to that curve. This necessarily incurs approximation, because the offset to a NURBS curve is not in general a NURBS curve, and thus contradicts the STEP-NC philosophy of using exact CAD geometry to drive manufacturing processes [22, 37]. The focus of this study is therefore on feedrate modulation as a means to achieve accurate and efficient execution of toolpaths specified explicitly as the offsets to a known, exact planar part geometry. It should be noted that the proposed methodology is specific to this context, although it may be possible to adapt it to other machining contexts.

Trimmed offsets inevitably exhibit tangent discontinuities, that may incur significant contour errors and machine vibrations if one attempts to traverse them at high feedrates. A strategy to accurately negotiate offset trim points is therefore a key element of the feedrate modulation scheme. Modulation of the feedrate is also desirable in concave high-curvature regions that do not necessitate offset trimming. In such regions, for a constant spindle speed and depth of cut, a fixed feedrate of the tool center can incur large deviations in the spacing of tool/part contact points at equal time intervals, resulting in large variation in the chip load (i.e., chip thickness) and machining forces. On the other hand, a variable feedrate that (approximately) achieves a constant chip load incurs high rates of acceleration/deceleration at the tool center. An approach that balances these two competing effects is clearly desirable.

The remainder of this paper is organized as follows. After reviewing some fundamental properties of trimmed planar offset curves in Section 2, the key advantages of Pythagorean–hodograph (PH) curves in the present context are summarized in Section 3. The feedrate modulation algorithms that facilitate accurate tracking of trim points and high-curvature concave regions are then developed in Section 4. These algorithms incorporate a number of adjustable parameters that can be used to balance the competing demands of tracking accuracy, suppression of machining force variations, and total execution time. Section 5 describes the implementation of the algorithms on a 3-axis CNC mill with an open-architecture controller and illustrates their performance using real-time data obtained from several experiments. Finally, in Section 6 we summarize the principal results of the present study, and discuss possible further developments of the feedrate modulation strategy.

2 Trimmed offset curves

We review here some basic properties of untrimmed and trimmed offset curves relevant to the present context (see [8, 17, 18, 32] for further details).

Consider a part shape defined by a closed planar contour C, comprising a sequence of curve segments $\mathbf{r}_i(\xi) = (x_i(\xi), y_i(\xi))$, $\xi \in [0,1]$ for $i = 1, \ldots, N$. These segments meet end-to-end with (at least) point continuity, such that C bounds a simply-connected domain, and the parameterization is assumed to be such that C has an anti-clockwise orientation. The *nodal points* of C are the junctures of its individual segments,

$$\mathbf{q}_i = \mathbf{r}_i(1) = \mathbf{r}_{i+1}(0)\,, \quad i = 1, \ldots, N-1$$

and

$$\mathbf{q}_N = \mathbf{r}_N(1) = \mathbf{r}_1(0)\,,$$

the index i being interpreted cyclically (i.e., $i = N+1$ is replaced by $i = 1$).

With $\mathbf{z}$ being a unit vector orthogonal to the plane, the unit *tangent* and *normal* vectors and the *curvature* on segment $\mathbf{r}_i(\xi)$ are defined [36] by

$$\mathbf{t}_i(\xi) = \frac{\mathbf{r}_i'(\xi)}{|\,\mathbf{r}_i'(\xi)\,|}\,, \qquad \mathbf{n}_i(\xi) = \mathbf{t}_i(\xi) \times \mathbf{z}\,,$$

$$\kappa_i(\xi) = \frac{[\,\mathbf{r}_i'(\xi) \times \mathbf{r}_i''(\xi)\,] \cdot \mathbf{z}}{|\,\mathbf{r}_i'(\xi)\,|^3}\,. \tag{1}$$

Note that $\mathbf{n}_i(\xi)$ points locally to the *right* of $\mathbf{t}_i(\xi)$, and $\kappa_i(\xi)$ is negative or positive when $\mathbf{n}_i(\xi)$ points toward or away from the center of curvature. If $\mathbf{t}_i(1) = \mathbf{t}_{i+1}(0)$, the nodal point $\mathbf{q}_i$ is *tangent-continuous*. A nodal point that is not tangent-continuous amounts to a curvature impulse, since the tangent and normal exhibit finite instantaneous rotations at such points.

The *untrimmed offset* at signed distance d to the curve segment $\mathbf{r}_i(\xi)$ is the locus defined by

$$\mathbf{r}_{d,i}(\xi) = \mathbf{r}_i(\xi) + d\,\mathbf{n}_i(\xi)\,, \quad \xi \in [0,1]\,. \tag{2}$$

This defines an *interior* or *exterior* offset to $\mathbf{r}_i(\xi)$ according to whether d is negative or positive. However, the untrimmed offset to the entire contour C is not simply the union of the offsets to all of the individual curve segments. If $\mathbf{q}_i$ is a tangent-continuous nodal point, the segments $\mathbf{r}_i(\xi)$ and $\mathbf{r}_{i+1}(\xi)$ have contiguous untrimmed offsets, i.e., $\mathbf{r}_{d,i}(1) = \mathbf{r}_{d,i+1}(0)$. However, if $\mathbf{q}_i$ is not tangent-continuous, the untrimmed offsets are not contiguous.

Let $\Delta\theta_i \in (-\pi, +\pi)$ be the finite rotation mapping $\mathbf{n}_i(1)$ onto $\mathbf{n}_{i+1}(0)$ at a tangent-discontinuous nodal point $\mathbf{q}_i$, satisfying

$$\cos\Delta\theta_i = \mathbf{n}_i(1)\cdot\mathbf{n}_{i+1}(0),\ \ \sin\Delta\theta_i = [\mathbf{n}_i(1)\times\mathbf{n}_{i+1}(0)]\cdot\mathbf{z}\,, \quad (3)$$

with angles considered positive anti-clockwise and negative clockwise. Then $\mathbf{q}_i$ is *convex* or *concave*, relative to the offset distance d, according to whether $d\,\Delta\theta_i$ is positive or negative. A convex nodal point $\mathbf{q}_i$ incurs a "gap" between segments $\mathbf{r}_{d,i}(\xi)$ and $\mathbf{r}_{d,i+1}(\xi)$, that must be *filled* by a circular arc defined by the rotation of $d\,\mathbf{n}_i(1)$ onto $d\,\mathbf{n}_{i+1}(0)$ through angle $\Delta\theta_i$. On the other hand, a concave nodal point $\mathbf{q}_i$ incurs an "overlap" of $\mathbf{r}_{d,i}(\xi)$ and $\mathbf{r}_{d,i+1}(\xi)$, which results in a self-intersection loop (after connecting $d\,\mathbf{n}_i(1)$ and $d\,\mathbf{n}_{i+1}(0)$ by the appropriate circular arc) that must be *trimmed* off.

In addition to the tangent-discontinuous nodes of C, self-intersections of individual segments of the untrimmed offset may be incurred by subsegments of high negative curvature, satisfying $\kappa(\xi) < -1/d$. In such cases, the points on a subset $[\,\xi_l, \xi_r\,] \subseteq [\,0, 1\,]$ of $\mathbf{r}_{d,i}(\xi)$ are all at distance $< |d|$ from $\mathbf{r}_i(\xi)$, and these subsegments must also be deleted to obtain the trimmed offset.

The untrimmed offset has the property that each of its open subsegments delineated by parameter values that correspond to self-intersections is either entirely at distance $|d|$ from the curve C, or entirely at distance $< |d|$ from C [18]. The offset *trimming* process consists of identifying and discarding all the subsegments in the latter category. The remaining subsegments, organized in proper order, comprise one or more closed loops that constitute the *trimmed offset*, which is a gouge-free path for machining C with a tool of radius d.

Figure 1 illustrates the offset trimming process for a multi-segment planar curve C, involving trimming at both concave nodes and interior subsegments of high negative curvature. In the present study, we assume that the trimmed offset curve has been pre-determined, and we focus on specifying a feedrate variation along it that permits an accurate and efficient traversal.

It should be noted that *any* trimming of the untrimmed offset reflects an inability to precisely machine the desired shape with a tool of radius $r = |d|$. To avoid an "overcut" (or *gouging*), the trimmed offset ensures an "undercut" — concave portions of the shape where the radius of curvature is less than r will be rounded out by circular fillet arcs of radius r on the machined part. This departure from the nominal part shape may be considered desirable, to relieve stress concentration by "filleting" sharp features in the part geometry. Alternatively, a finish machining pass with a smaller tool may be performed to produce a final part closer in shape to the nominal geometry.

3 Pythagorean-hodograph curves

The trimmed offset feedrate modulation algorithms developed herein are, in principle, applicable to curves defined by general piecewise-analytic forms. However, Pythagorean–hodograph (PH) curves [14] are especially well-suited to the present context, on account of their distinctive properties:

- Unlike general polynomial or rational curves, PH curves possess *rational* offsets, that are exactly compatible with the prevailing representation schemes of CAD systems.
- The arc length of any PH curve subsegment can be exactly computed by simply evaluating a polynomial, rather than relying on an approximate numerical quadrature scheme.
- PH curves admit essentially exact real-time interpolator algorithms for feedrates dependent upon time, arc length, curvature, etc., through the analytic reduction of the interpolation integral.

A detailed treatment of the PH curves may be found in [14], and the references [4, 12, 16, 19, 20, 34] describe examples of their applications in real–time motion control. We outline only the most essential aspects here. A planar polynomial PH curve $\mathbf{r}(\xi) = (x(\xi), y(\xi))$ has the distinctive feature that its derivative $\mathbf{r}'(\xi) = (x'(\xi), y'(\xi))$ satisfies the Pythagorean condition

$$x'^2(\xi) + y'^2(\xi) = \sigma^2(\xi) \quad (4)$$

for some polynomial $\sigma(\xi)$, which defines the *parametric speed* of $\mathbf{r}(\xi)$—i.e., the derivative $\mathrm{d}s/\mathrm{d}\xi$ of arc length s with respect to the curve parameter ξ. The fact that $\sigma(\xi)$ is a just polynomial (not the square root of a polynomial) endows the PH curves with many attractive computational properties.

For a primitive curve—i.e., $\gcd(x'(\xi), y'(\xi)) = \text{constant}$—a sufficient and necessary condition for the satisfaction of Eq. 4 is that $x'(\xi)$ and $y'(\xi)$ must be expressible in terms of polynomials $u(\xi)$, $v(\xi)$ in the form

$$x'(\xi) = u^2(\xi) - v^2(\xi)\,, \quad y'(\xi) = 2\,u(\xi)v(\xi)\,.$$

This structure is embodied in the complex representation [13]—representing points (x, y) in the Euclidean plane by complex values $x + \mathrm{i}\,y$, a PH curve of degree $n = 2m + 1$ can be generated from a degree m complex polynomial

$$\mathbf{w}(\xi) = u(\xi) + \mathrm{i}\,v(\xi)$$

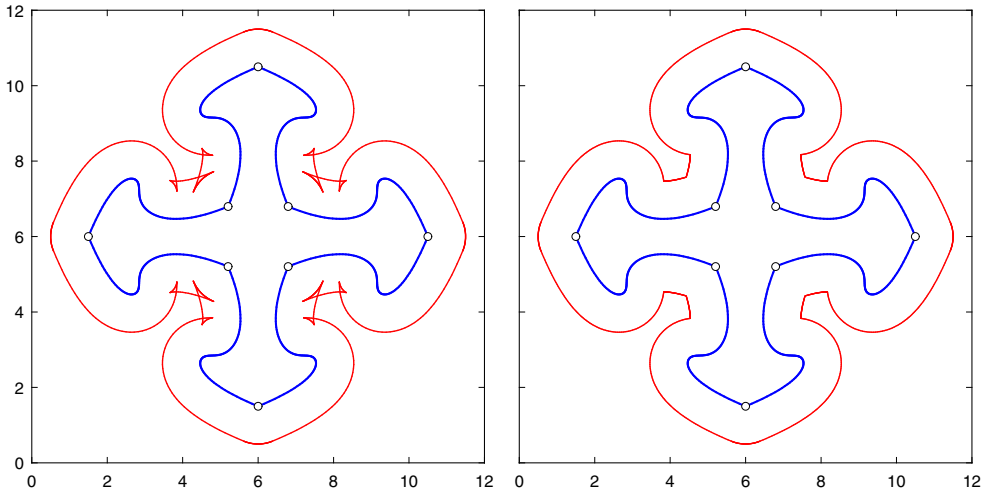

Fig. 1 Left: untrimmed offset to a multi-segment curve C, exhibiting self-intersection loops incurred by both concave nodal points between segments, and high-curvature concave regions within segments. Right: trimmed offset, obtained by deleting parts of the untrimmed offset at distance $< |d|$ from C. The x and y axes scales of the plots indicate the curve dimensions in inches

by integrating the expression

$$\mathbf{r}'(\xi) \;=\; \mathbf{w}^2(\xi)\,.$$

The tangent, normal, and the curvature of $\mathbf{r}(\xi)$ have a *rational* dependence on the curve parameter ξ, and may be expressed [14] in terms of $\mathbf{w}(\xi)$ as

$$\mathbf{t}(\xi) \;=\; \frac{\mathbf{w}^2(\xi)}{\sigma(\xi)}\,, \quad \mathbf{n}(\xi) \;=\; -\,\mathrm{i}\,\frac{\mathbf{w}^2(\xi)}{\sigma(\xi)}\,,$$

$$\kappa(\xi) \;=\; 2\,\frac{\mathrm{Im}(\overline{\mathbf{w}}(\xi)\mathbf{w}'(\xi))}{\sigma^2(\xi)}\,.$$

Since $\sigma(\xi)$ is a polynomial, the cumulative arc length function

$$s(\xi) \;=\; \int_0^{\xi} \sigma(t)\;\mathrm{d}t$$

is also a polynomial in ξ. Moreover, the offset curves

$$\mathbf{r}_d(\xi) \;=\; \mathbf{r}(\xi) \;+\; d\,\mathbf{n}(\xi)$$

at each distance d can be exactly represented as rational curves. For further details and algorithms to construct PH curves under a variety of geometrical constraints, we refer the reader to [14].

4 Feedrate modulation algorithm

The parametric speed $\sigma(\xi) \;=\; |\mathbf{r}'(\xi)|$ of a curve $\mathbf{r}(\xi)$ specifies the derivative $\mathrm{d}s/\mathrm{d}\xi$ of arc length s with the respect to the curve parameter ξ. Since the feedrate V is the rate of change $\mathrm{d}s/\mathrm{d}t$ of arc length with time, by use of the chain rule, we obtain

$$\frac{\mathrm{d}\xi}{\mathrm{d}t} \;=\; \frac{\mathrm{d}s}{\mathrm{d}t}\,\frac{\mathrm{d}\xi}{\mathrm{d}s} \;=\; \frac{V}{\sigma}\,. \tag{5}$$

This basic relationship governs the design of the *real-time interpolator*, a key component of CNC machine controllers. The function of the interpolator is to compute a *reference point* (commanded machine position) in each sampling interval δt of the servo system, from the path geometry and feedrate specified in the part program. The discrepancy between the reference point and actual machine location, measured by position encoders, defines the instantaneous position error, which is the basic feedback control signal. The present focus is on trimmed offsets to piecewise-smooth analytic curves, as specified by a set of parameter sub–domains for each of a sequence $\mathbf{r}_1(\xi), \ldots, \mathbf{r}_N(\xi)$ of curve segments that define a closed loop of counter-clockwise orientation.

4.1 Feedrate modulation at tangent discontinuities

Trim points on the trimmed offset path are in general tangent-discontinuous, whether they are incurred by concave tangent-discontinuous nodes between curve segments, or concave regions of high curvature within a single segment. Attempting to traverse a trimmed offset path at a constant feedrate can incur unacceptable tracking inaccuracies or machine vibrations at such points. To circumvent this, it is necessary to decelerate on approaching trim points, and accelerate back to the nominal feedrate on departing from them.

Consider two consecutive trimmed offset segments

$$\mathbf{r}_{d,i}(\xi)\,, \quad \xi \in [\xi_{i,0}, \xi_{i,1}], \mathbf{r}_{d,i+1}(\xi)\,, \quad \xi \in [\xi_{i+1,0}, \xi_{i+1,1}]$$

with $[\,\xi_{i,0}, \xi_{i,1}\,] \subset [\,0, 1\,]$ and $[\,\xi_{i+1,0}, \xi_{i+1,1}\,] \subset [\,0, 1\,]$. They may arise as offsets from a single segment or two distinct segments of the curve C, and they meet at the tangent-discontinuous juncture $\mathbf{r}_{d,i}(\xi_{i,1}) \;=\; \mathbf{r}_{d,i+1}(\xi_{i+1,0})$. To accurately negotiate such points, a modulation factor is applied that smoothly reduces the feedrate on approach, and smoothly restores it on departure.

Consider the approach phase. If $s(\xi)$ is the arc-length function[1] for the segment of C that generates $\mathbf{r}_{d,i}(\xi)$, the

[1] For PH curves, $s(\xi)$ is a polynomial and can be exactly evaluated.

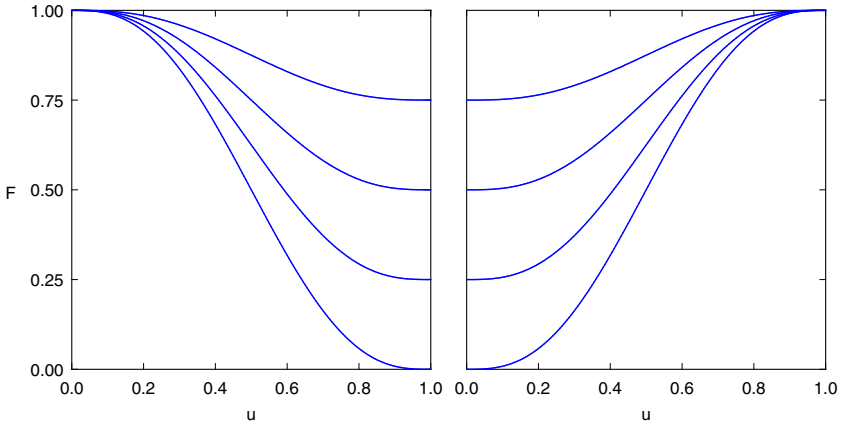

Fig. 2 The feedrate modulation functions (7) and (10) with the reduction factors $f = 0.75$, 0.50, 0.25, 0.00 for (left) the deceleration phase, and (right) the acceleration phase, defined by the coefficients (8) and (11), respectively

total arc length on C associated with the trimmed offset segment is $\Delta s = s(\xi_{i,1}) - s(\xi_{i,0})$. We apportion a fraction λ of Δs to the deceleration phase and stipulate that the feedrate be reduced from its nominal value V to $f\,V$ for some fraction $0 \le f \le 1$. Associating with each $\xi \in [\,\xi_{i,0}, \xi_{i,1}\,]$ the fractional arc-length parameter

$$u = \frac{s(\xi) - s(\xi_{i,0})}{\Delta s} \in [\,0, 1\,], \tag{6}$$

a smooth feedrate decrease from V to $f\,V$ over the distance $\lambda\Delta s$ is achieved through multiplying V by the quintic polynomial

$$F(u) = \sum_{i=0}^{5} f_i \binom{5}{i} \frac{(1-u)^{5-i}(u-1+\lambda)^i}{\lambda^5} \tag{7}$$

with Bernstein coefficients

$$f_0 = f_1 = f_2 = 1 \quad \text{and} \quad f_3 = f_4 = f_5 = f\,. \tag{8}$$

This polynomial is characterized by the properties

$$F(0) = 1\,, \quad F'(0) = F''(0) = 0$$
$$F(1) = f\,, \quad F'(1) = F''(1) = 0\,,$$

which ensure that the feedrate modulation exhibits C^2 continuity.

Upon completing segment $\mathbf{r}_{d,i}(\xi)$ and entering segment $\mathbf{r}_{d,i+1}(\xi)$, a similar strategy is employed to increase the feedrate from $f\,V$ to V. If $s(\xi)$ is the arc-length function for the segment of C that generates $\mathbf{r}_{d,i+1}(\xi)$, we compute the total arc length $\Delta s = s(\xi_{i+1,1}) - s(\xi_{i+1,0})$, and apportion a fraction λ of it to the acceleration phase. Defining

$$u = \frac{s(\xi) - s(\xi_{i+1,0})}{\Delta s} \in [\,0, 1\,], \tag{9}$$

a smooth feedrate increase from $f\,V$ to V over the distance $\lambda\Delta s$ is achieved through multiplying V by the quintic polynomial

$$F(u) = \sum_{i=0}^{5} f_i \binom{5}{i} \frac{(\lambda-u)^{5-i}u^i}{\lambda^5} \tag{10}$$

with Bernstein coefficients

$$f_0 = f_1 = f_2 = f \quad \text{and} \quad f_3 = f_4 = f_5 = 1\,. \tag{11}$$

This ensures a C^2 increase in feedrate from $f\,V$ to V over distance $\lambda\Delta s$, since the polynomial (10) satisfies

$$F(0) = f\,, \quad F'(0) = F''(0) = 0$$
$$F(1) = 1\,, \quad F'(1) = F''(1) = 0\,.$$

Figure 2 illustrates the functions (7) and (10) used to modulate the feedrate at tangent discontinuities, for both the deceleration and acceleration phases, and various values of the feedrate reduction factor f.

The two parameters λ and f, which determine the extent and magnitude of the feed deceleration/acceleration phases, can be specified individually at each tangent discontinuity in accordance with its severity, or to ensure that physical bounds on deceleration/acceleration rates are not exceeded. Clearly, for trimmed offset segments with tangent discontinuities at both ends, the sum of the λ values at these ends cannot exceed 1.

4.2 Curvature-dependent modulation of feedrate

For a smooth plane curve segment $\mathbf{r}(\xi)$, $\xi \in [\,0, 1\,]$ with curvature $\kappa(\xi)$, the offset $\mathbf{r}_d(\xi)$ at distance d has [17] the curvature

$$\kappa_d(\xi) = \frac{\kappa(\xi)}{|\,1 + \kappa(\xi)\,d\,|}\,.$$

Hence, we have $|\kappa_d(\xi)| > |\kappa(\xi)|$ when $-1 < \kappa(\xi)\,d < 0$, and $|\kappa_d(\xi)| < |\kappa(\xi)|$ when $\kappa(\xi)\,d > 0$. These cases identify *convex* and *concave* segments of $\mathbf{r}(\xi)$, relative to the offset distance d, respectively. When $\kappa(\xi) = -1/d$, the point $\mathbf{r}_d(\xi)$ is a *cusp* on the offset, and a concave segment with $\kappa(\xi) < -1/d$ incurs a self-intersection loop on $\mathbf{r}_d(\xi)$, that must be trimmed off.

For a constant tool spindle speed and depth of cut, executing a strongly-curved offset path at constant feedrate leads to an uneven spacing of tool/part contact points,

leading to significant chip load variations that may cause tool chatter or poor machined surface finish. This can be remedied by specifying the feedrate in a manner that yields uniform spacing of the tool/part contact points, but large variations in the tool center speed may then be incurred—which, in conjunction with the offset path curvature, imply large acceleration magnitudes (see Fig. 3). A method for balancing the conflicting demands of variations in chip load and acceleration is therefore clearly desirable.

A curve $\mathbf{r}(\xi)$ and its offset $\mathbf{r}_d(\xi)$ at distance d satisfy [17] the relation

$$\mathbf{r}_d'(\xi) \;=\; [\,1+\kappa(\xi)\,d\,]\,\mathbf{r}'(\xi)\,,$$

where $\kappa(\xi)$ is the curvature of $\mathbf{r}(\xi)$. Hence, the parametric speeds

$$\sigma(\xi) \;=\; |\mathbf{r}'(\xi)| \;=\; \frac{\mathrm{d}s}{\mathrm{d}\xi} \quad \text{and} \quad \sigma_d(\xi) \;=\; |\mathbf{r}_d'(\xi)| \;=\; \frac{\mathrm{d}s_d}{\mathrm{d}\xi}\,, \tag{12}$$

where s and s_d denote arc length along $\mathbf{r}(\xi)$ and $\mathbf{r}_d(\xi)$, are related by

$$\sigma_d(\xi) \;=\; |\,1+\kappa(\xi)\,d\,|\,\sigma(\xi)\,. \tag{13}$$

Since the speeds of points that move along $\mathbf{r}(\xi)$ and $\mathbf{r}_d(\xi)$ are defined by the time derivatives

$$V \;=\; \frac{\mathrm{d}s}{\mathrm{d}t} \quad \text{and} \quad V_d \;=\; \frac{\mathrm{d}s_d}{\mathrm{d}t}\,, \tag{14}$$

we have

$$V_d \;=\; \frac{\mathrm{d}s_d}{\mathrm{d}s}\,V \;=\; \frac{\mathrm{d}s_d}{\mathrm{d}\xi}\frac{\mathrm{d}\xi}{\mathrm{d}s}\,V \;=\; \frac{\sigma_d(\xi)}{\sigma(\xi)}\,V \;=\; |\,1+\kappa(\xi)\,d\,|\,V\,. \tag{15}$$

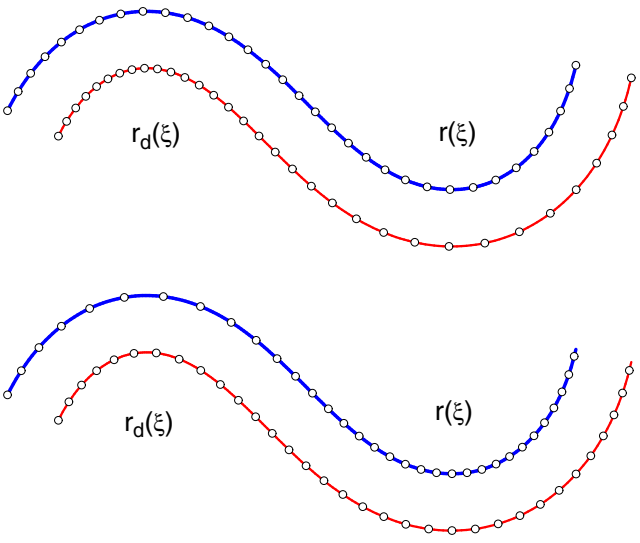

Fig. 3 Upper: a uniform speed along the curve $\mathbf{r}(\xi)$ induces a non–uniform speed along the offset curve $\mathbf{r}_d(\xi)$. Lower: conversely, a uniform speed along the offset curve $\mathbf{r}_d(\xi)$ induces a non-uniform speed along the curve $\mathbf{r}(\xi)$

Here, V can be interpreted as the speed of the tool/part contact point, while V_d represents the speed of the tool center (moving on the offset path).

To achieve a constant speed V of the tool/part contact point, and thus an (approximately) constant chip load, the tool center must have the speed V_d specified by Eq. 15. When $\kappa(\xi) = 0$, we have $V_d = V$, but when $\mathbf{r}(\xi)$ has strong negative and positive curvatures, the factor $|\,1+\kappa(\xi)\,d\,|$ in Eq. 15 will incur large deviations about the constant value V. In such cases, there is a fundamental conflict between the desire to suppress machining force fluctuations and the need to avoid large acceleration/deceleration rates along the tool path.

For a constant speed V of the tool/part contact point, we must use V_d as the speed of the tool center, and we have

$$V_d \;=\; \frac{\mathrm{d}s_d}{\mathrm{d}t} \;=\; \frac{\mathrm{d}s_d}{\mathrm{d}\xi}\frac{\mathrm{d}\xi}{\mathrm{d}t} \;=\; \sigma_d\,\frac{\mathrm{d}\xi}{\mathrm{d}t}\,,$$

and using Eqs. 13 and 15, we obtain

$$\frac{\mathrm{d}\xi}{\mathrm{d}t} \;=\; \frac{V_d}{\sigma_d} \;=\; \frac{V}{\sigma(\xi)}\,. \tag{16}$$

On the other hand, to achieve a constant speed V of the tool center on the offset path, we have

$$V \;=\; \frac{\mathrm{d}s_d}{\mathrm{d}t} \;=\; \frac{\mathrm{d}s_d}{\mathrm{d}\xi}\frac{\mathrm{d}\xi}{\mathrm{d}t} \;=\; \sigma_d\,\frac{\mathrm{d}\xi}{\mathrm{d}t}\,,$$

and hence

$$\frac{\mathrm{d}\xi}{\mathrm{d}t} \;=\; \frac{V}{\sigma_d} \;=\; \frac{V}{|\,1+\kappa(\xi)\,d\,|\,\sigma(\xi)}\,. \tag{17}$$

Equations 16 and 17 define the time derivatives of the common parameter ξ of the curve $\mathbf{r}(\xi)$ and its offset $\mathbf{r}_d(\xi)$, according to whether we stipulate (1) a constant speed V of the tool/part contact point, or (2) a constant speed V of the tool center along the offset path, respectively. The latter can incur large variations in chip load, and the former large variations in the acceleration of the tool center. To balance these competing effects, we consider for $0 \le w \le 1$ the weighted combination of Eqs. 16 and 17, namely

$$\frac{\mathrm{d}\xi}{\mathrm{d}t} \;=\; (1-w)\,\frac{V}{\sigma(\xi)} \;+\; w\,\frac{V}{|\,1+\kappa(\xi)\,d\,|\,\sigma(\xi)}\,. \tag{18}$$

The cases $w = 0$ and $w = 1$ correspond to Eqs. 16 and 17, respectively. The choice of the weight w allows one to place greater emphasis on minimizing the variations in chip load or in tool acceleration, according to the requirements of specific applications. Equation 18 can be re-formulated as

$$\frac{\mathrm{d}\xi}{\mathrm{d}t} \;=\; \frac{V}{\sigma_w(\xi)}\,, \tag{19}$$

in terms of the "weighted parametric speed" defined by

$$\sigma_w(\xi) \;=\; \frac{|\,1+\kappa(\xi)\,d\,|}{(1-w)\,|\,1+\kappa(\xi)\,d\,|+w}\,\sigma(\xi)\,. \tag{20}$$

The free parameters λ, f, w in the feedrate modulation methodology can be adjusted in accordance with the circumstances and requirements of specific machining applications, including tool radius, desired chip load and machined surface finish, specific cutting energy of the workpiece material, etc.

4.3 Real-time interpolator algorithm

Equations 19 and 20 form the basis of a real-time interpolator algorithm that achieves a fixed speed V of the tool/part contact point ($w = 0$); of the tool center along the offset path ($w = 1$); or for a linear "blend" of these two conditions ($0 < w < 1$). Combining this with the feedrate modulation factors (7) and (10) associated with the tangent discontinuities of the trimmed offset, we set

$$\frac{\mathrm{d}\xi}{\mathrm{d}t} = F(u)\,\frac{V}{\sigma_w(\xi)}\,, \tag{21}$$

where the dependence of u on ξ is defined by Eqs. 6 or 9, and the polynomial $F(u)$ is specified by either (7) and (8) or (10) and (11), for the deceleration and acceleration phases, respectively.

For a sampling interval δt, a first-order real-time interpolator based on Eq. 21 yields the parameter value $\xi_{k+1} = \xi_k + \delta\xi_k$ for the offset curve reference point at time $(k+1)\delta t$ from the parameter value ξ_k at time $k\delta t$, where

$$\delta\xi_k = F(u_k)\frac{V}{\sigma_w(\xi_k)}\,\delta t\,, \tag{22}$$

and u_k is given by Eqs. 6 or 9 evaluated at $\xi = \xi_k$. This first-order interpolator is commonly used [3, 25, 29, 41] and is sufficiently accurate for applications employing small sampling intervals δt and modest feedrates V. When greater accuracy is desired, the first-order expansion (22) may be improved by the inclusion of second and third order terms in δt [21], or analytic integration of the relation (5) in the case of Pythagorean–hodograph curves [19].

5 Implementation and experimental results

To assess its performance, the trimmed offset feedrate modulation algorithm was implemented on a 3-axis CNC mill governed by an open-architecture software controller, and experiments were run for various combinations of the user-specified parameters λ, f, w using the test curve illustrated in Fig. 1. The dimensions in Fig. 1 are in inches, and the specified offset distance is $d = 1$ in. The test curve consists of eight quintic PH curve segments, and the chosen d value incurs trimming at both concave interior nodes, and concave high-curvature regions within individual PH curve segments.

Real-time data from the axis position encoders is stored in memory during each run, and post-processed to assess performance measures such as actual feedrate achieved, acceleration magnitude, and contour error (i.e., the normal deviation of the actual executed path executed from the exact offset path).

5.1 Open-architecture software controller

The CNC milling machine used for the experiments is illustrated in Fig. 4. The machine controller is based on the MDSI OpenCNC open-architecture software, which allows incorporation of customized real-time motion control algorithms written in the C++ language. The controller runs on a commercial PC with a modest 500 MHz CPU and uses a sampling frequency $f = 1024$ Hz, corresponding to a sampling interval $\delta t = 1/f \approx 0.001$ s. The software modifications were implemented entirely within the real-time interpolator, which generates a reference point (i.e., commanded machine position) in each sampling interval of the servo system, from the trimmed offset path geometry and the modulated feedrate variation along it.

5.2 Analysis of experimental results

The experiments were performed on the multi-segment test curve illustrated in Fig. 1, which exhibits both concave tangent-discontinuous nodes and high-curvature regions within individual segments. The nodal angles (3) are a measure of the severity of the tangent discontinuities, and the parameters λ and f can both be exploited to control the deceleration/acceleration rates in traversing such nodes. Although individual λ values can be assigned to each node, to maintain a reasonable number of parameter combinations we choose here to fix the arc length fraction at $\lambda = 0.25$, and

Fig. 4 3-axis CNC mill governed by the OpenCNC software controller

Table 1 Total trimmed offset path traversal times for runs with weight values $w = 0.0, 0.5, 1.0$ and the feedrate reduction factors $f = 0.25, 0.50, 0.75, 1.00$

	$f = 0.25$	$f = 0.50$	$f = 0.75$	$f = 1.00$
$w = 0.0$	12.67 s	10.23 s	9.20 s	8.60 s
$w = 0.5$	14.44 s	11.52 s	10.28 s	9.56 s
$w = 1.0$	24.27 s	18.27 s	15.69 s	14.19 s

Table 2 Maximum measured contour error for runs with the weight values $w = 0.0, 0.5, 1.0$ and the feedrate reduction factors $f = 0.25, 0.50, 0.75, 1.00$

	$f = 0.25$	$f = 0.50$	$f = 0.75$	$f = 1.00$
$w = 0.0$	0.0016 in	0.0071 in	0.0260 in	0.1296 in
$w = 0.5$	0.0016 in	0.0032 in	0.0072 in	0.0186 in
$w = 1.0$	0.0014 in	0.0025 in	0.0036 in	0.0050 in

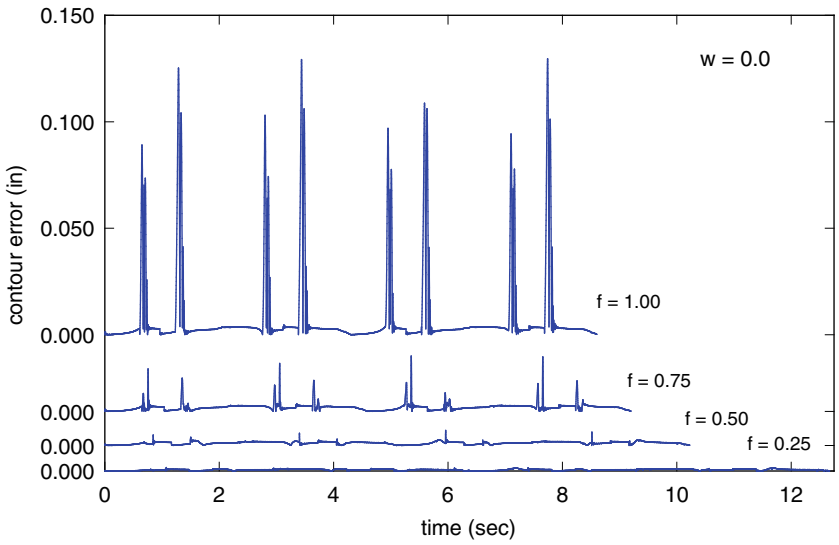

Fig. 5 Variation of contour error with time along the trimmed offset path shown in Fig. 1, for the cases $w = 0.0$ with $f = 0.25, 0.50, 0.75, 1.00$. The plots are drawn to the same scale, but are displaced vertically for clarity

Table 3 Maximum measured feedrates for runs with the weight values $w = 0.0, 0.5, 1.0$ and the feedrate reduction factors $f = 0.25, 0.50, 0.75, 1.00$

	$f = 0.25$	$f = 0.50$	$f = 0.75$	$f = 1.00$
$w = 0.0$	707.5 in/min	870.4 in/min	1213.2 in/min	1341.7 in/min
$w = 0.5$	427.0 in/min	506.6 in/min	647.4 in/min	798.7 in/min
$w = 1.0$	222.9 in/min	221.6 in/min	226.2 in/min	241.7 in/min

Table 4 Maximum acceleration magnitudes for runs with the weight values $w = 0.0, 0.5, 1.0$ and the feedrate reduction factors $f = 0.25, 0.50, 0.75, 1.00$

	$f = 0.25$	$f = 0.50$	$f = 0.75$	$f = 1.00$
$w = 0.0$	332.8 in/s^2	643.2 in/s^2	707.7 in/s^2	962.0 in/s^2
$w = 0.5$	331.3 in/s^2	465.3 in/s^2	667.7 in/s^2	705.3 in/s^2
$w = 1.0$	336.5 in/s^2	299.9 in/s^2	416.9 in/s^2	560.9 in/s^2

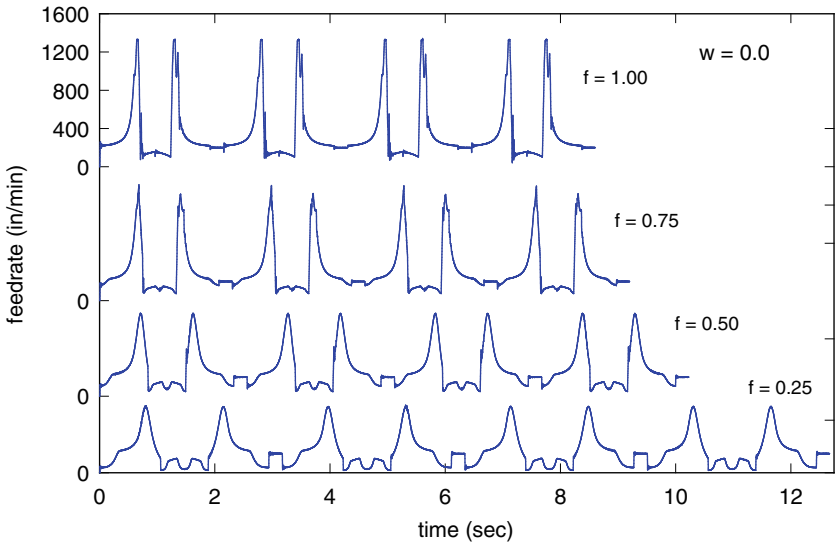

Fig. 6 Variation of measured feedrate along the trimmed offset path shown in Fig. 1, for the cases $w = 0.0$ with $f = 0.25, 0.50, 0.75, 1.00$. The four plots are drawn to the same scale, but are displaced vertically for clarity

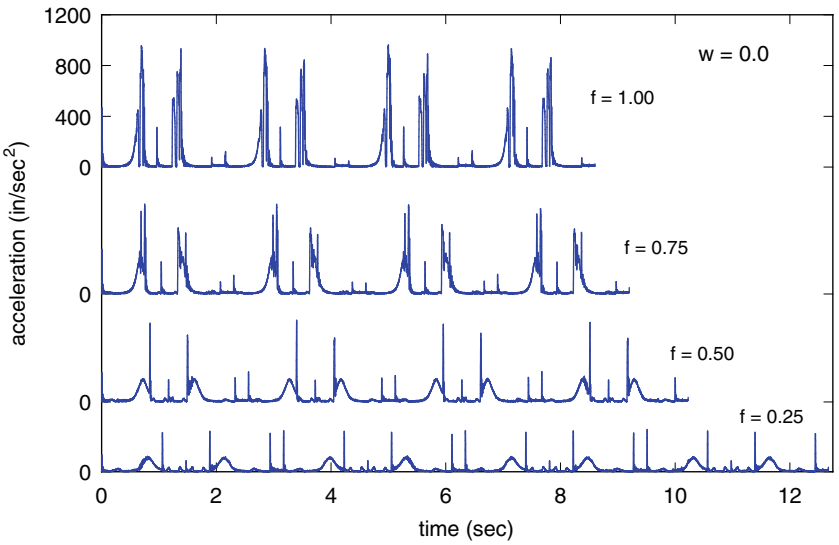

Fig. 7 Variation of acceleration magnitude along the trimmed offset path shown in Fig. 1 for the cases $w = 0.0$ with $f = 0.25, 0.50, 0.75, 1.00$. The four plots are drawn to the same scale, but are displaced vertically for clarity

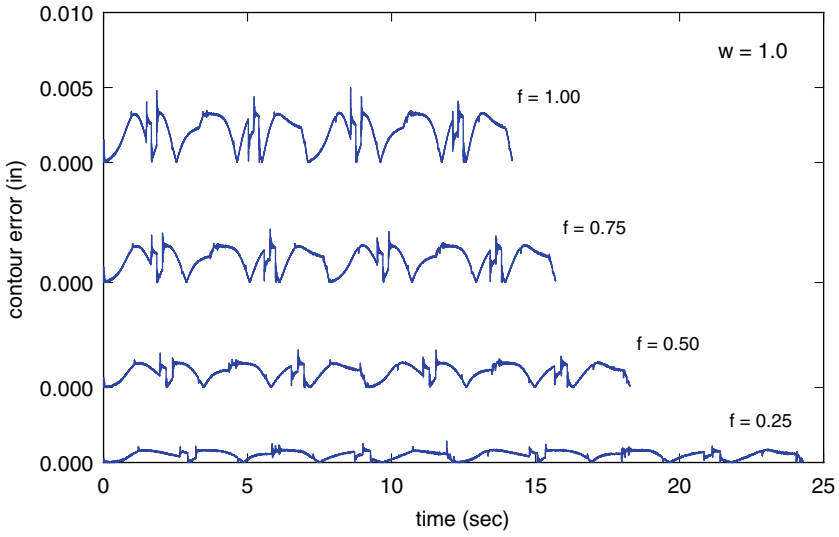

Fig. 8 Variation of contour error with time along the trimmed offset path shown in Fig. 1, for the cases $w = 1.0$ with $f = 0.25, 0.50, 0.75, 1.00$. The plots are drawn to the same scale, but are displaced vertically for clarity

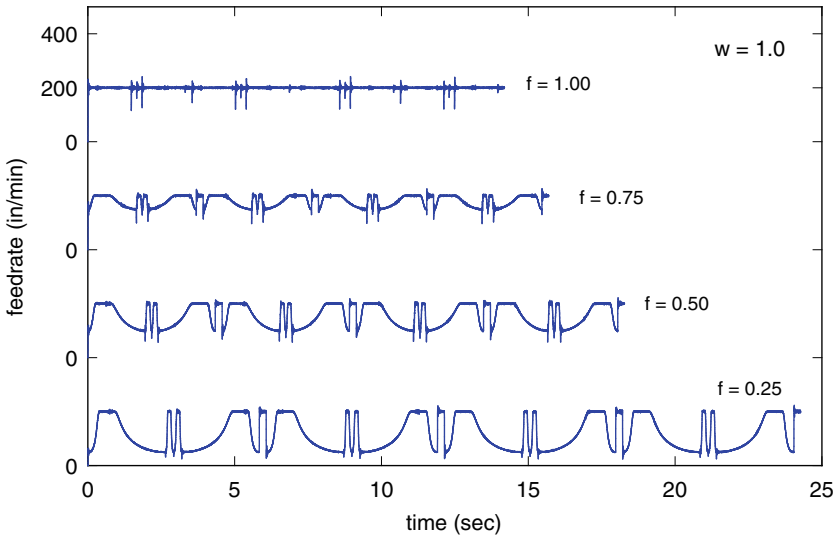

Fig. 9 Variation of measured feedrate along the trimmed offset path shown in Fig. 1, for the cases $w = 1.0$ with $f = 0.25, 0.50, 0.75, 1.00$. The four plots are drawn to the same scale, but are displaced vertically for clarity

vary the feedrate reduction factor f instead. Experiments were run with values $f = 0.25, 0.5, 0.75, 1.0$ in conjunction with the weights $w = 0.0, 0.5, 1.0$ in expressions (18)–(20), and the nominal feedrate $V = 200$ in/min was used in all instances.

The experimental results of primary interest, in terms of their dependence on f and w, include the following: (1) total path traversal time; (2) maximum path contour error; (3) correct realization of the feedrate modulation; and (4) maximum acceleration magnitude. Table 1 lists the measured path traversal times. As expected, the fastest time of 8.60 s is obtained with $w = 0$ and $f = 1$ (i.e., constant speed of the tool/part contact point with no feedrate reduction at tangent discontinuities), while the slowest time of 24.27 s is obtained with $w = 1$ and $f = 0.25$ (i.e., constant speed of the tool center along the offset path, with a 75% feedrate reduction at tangent discontinuities).

The measured maximum contour errors, listed in Table 2 and illustrated in Figs. 5, 8, and 11, are inversely correlated with the path traversal times: the fastest case ($w = 0$ and $f = 1$) incurs an unacceptable maximum contour error of 0.1296 in, while the slowest case ($w = 1$ and $f = 0.25$) exhibits a very small maximum contour error of 0.0014 in. The corresponding maximum feedrates and acceleration magnitudes are listed in Tables 3 and 4.

As seen in Fig. 6, the case $w = 0$ of a constant speed for the tool/part contact point produces peak tool center feedrates > 1200 in/min, exceeding the nominal 200 in/min feedrate by a factor greater than six, if no feedrate reduction is imposed at offset trim points ($f = 1$), and the peak accelerations seen in Fig. 7 are correspondingly very high. These high speeds and rates of acceleration are the primary cause of the large contour errors when $f = 1$. As evident in Figs. 5, 6, and 7, the use of deceleration/acceleration phases

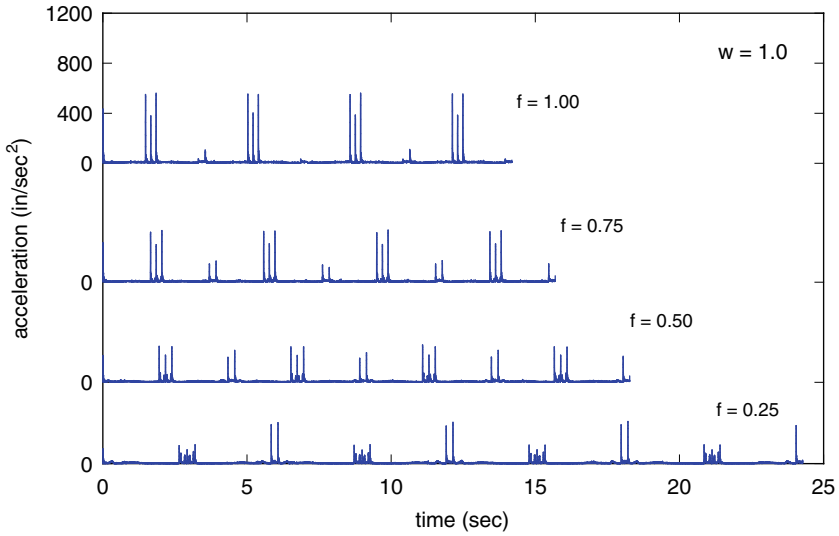

Fig. 10 Variation of acceleration magnitude along the trimmed offset path shown in Fig. 1 for the cases $w = 1.0$ with $f = 0.25, 0.50, 0.75, 1.00$. The four plots are drawn to the same scale, but are displaced vertically for clarity

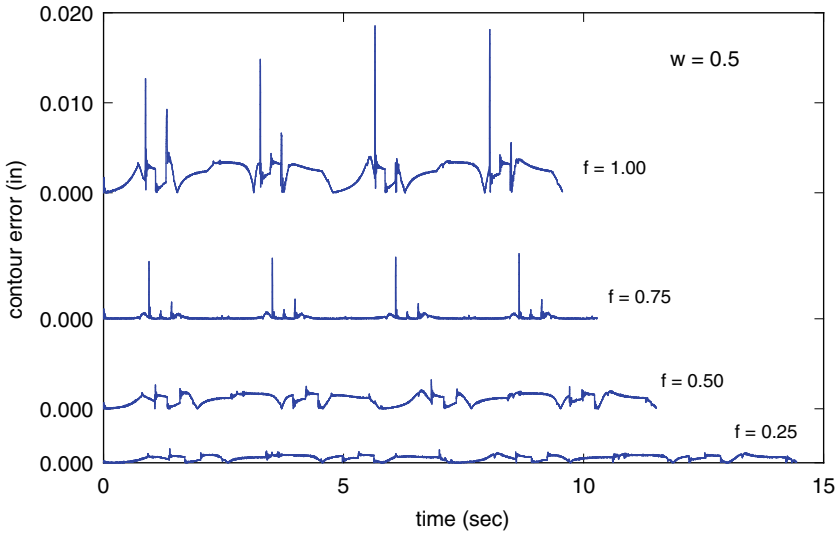

Fig. 11 Variation of contour error with time along the trimmed offset path shown in Fig. 1, for the cases $w = 0.5$ with $f = 0.25, 0.50, 0.75, 1.00$. The plots are drawn to the same scale, but are displaced vertically for clarity

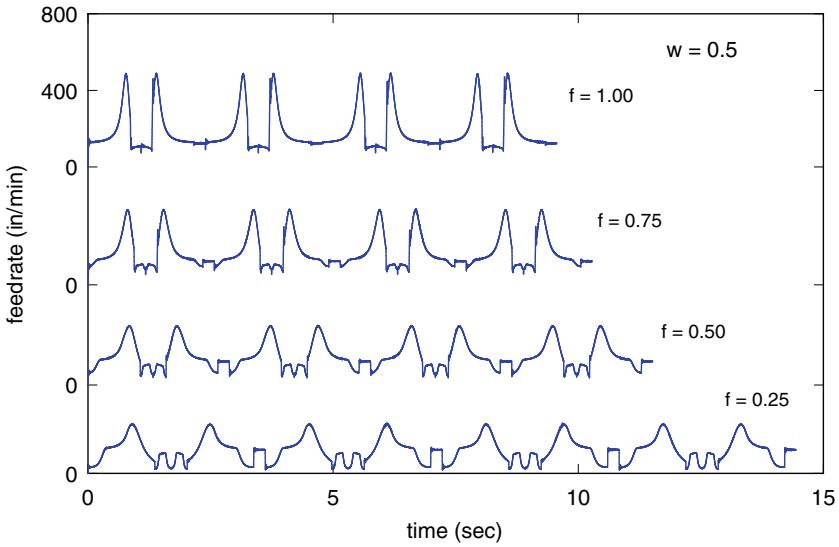

Fig. 12 Variation of measured feedrate along the trimmed offset path in Fig. 1, for the cases $w = 0.5$ with $f = 0.25, 0.50, 0.75, 1.00$. The four plots are drawn to the same scale, but are displaced vertically for clarity

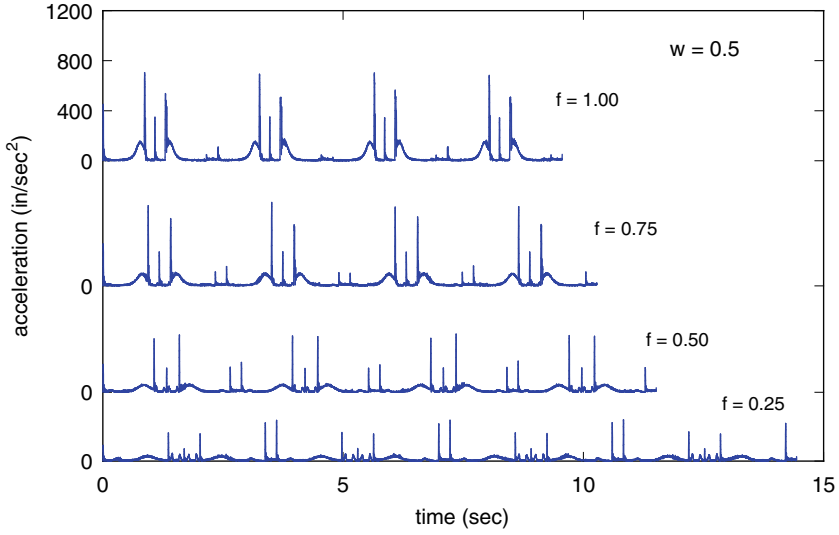

Fig. 13 Variation of acceleration magnitude along the trimmed offset path shown in Fig. 1 for the cases $w = 0.5$ with $f = 0.25, 0.50, 0.75, 1.00$. The four plots are drawn to the same scale, but are displaced vertically for clarity

in negotiating offset trim points when $f = 1$ substantially reduces the peak contour error, feedrate, and acceleration, especially for $f \leq 0.5$, at the cost of a somewhat greater traversal time. To maintain acceptable accuracy, feedrate modulation is clearly essential in the presence of offset trim points and high-curvature concave regions when using the feedrate (15) corresponding to a constant chip load, especially for high-speed machining [26, 35, 40].

The case $w = 1$ of a constant speed of the tool center along the trimmed offset path produces a much smoother motion (with lower peak feedrates and acceleration magnitudes) and smaller contour errors, as evident in Tables 2, 3 and 4 and Figs. 8, 9, and 10 (note the different vertical scales in these plots, compared to Figs. 5, 6, and 7), especially for feedrate reduction factors $f \leq 0.5$. As previously emphasized, however, a constant tool speed along the offset path may incur large variation in the spacing of tool/part contact points (i.e., chip load) and hence large machining force fluctuations and machine vibrations.

Finally, we consider the intermediate case $w = 0.5$ in Eqs. 18–20, representing a balance between the two extremes of strong feedrate variation ($w = 0$) and strong chip load variation ($w = 1$). The results for the $w = 0.5$ runs are listed in Tables 2, 3 and 4, and are illustrated in Figs. 11, 12, and 13. It is seen that, at corresponding f values, the traversal times are only modestly slower than those for $w = 0$, and significantly faster than those for $w = 1$. On the other hand, the maximum contour errors are much smaller than those for $w = 0$, and quite comparable to those for $w = 1$ when $f \leq 0.5$. In Tables 3 and 4 and Figs. 12 and 13, we see that these runs also maintain reasonable maximum feedrates and acceleration magnitudes, especially for $f \leq 0.5$.

6 Conclusion

Accurate and efficient execution of trimmed offset paths is essential in gouge-free machining of complex shapes with a tool of specified radius. These paths often exhibit tangent discontinuities and strong curvature variations, even for smooth part shapes with mild curvature variation. Consequently, continuous modulation of feedrate on trimmed offset paths is essential to ensuring precise tracking in conjunction with efficient traversal times.

Two key aspects of the feedrate modulation scheme have been identified in this study: (i) the need for deceleration/acceleration phases associated with tangent-discontinuous offset points, resulting from the trimming process; and (ii) the need to balance the competing goals of minimizing large variations in chip loads and tool accelerations. To address aspect (i), arc-length fractions λ of the segments that meet at a tangent-discontinuous node were apportioned to deceleration/acceleration phases, with a C^2 modulation function defined on them to smoothly reduce the feedrate from the nomimal value V to $f\,V$ and then smoothly increase it back to V, for some fraction $0 \leq f \leq 1$.

To address aspect (ii), a weight $w \in [0, 1]$ was introduced such that to the values $w = 0$ and $w = 1$ correspond, respectively, the extremes of a constant chip load, and a constant feedrate of the tool center along the offset path. By formulating a real-time interpolator algorithm specified through a weighted sum of these extremes, a feedrate modulation scheme that "balances" their competing effects was formulated for w values between 0 and 1.

The proposed methodology is most directly applicable to finish-machining cuts that involve a fixed depth of cut and constant spindle speed. However, the user-specified parameters λ, f, w allow it to be fine-tuned to many other application contexts. Experiments from an implementation on a 3-axis CNC mill with an open-architecture controller show that the feedrate modulation scheme achieves excellent results in simultaneously minimizing path contour error, suppressing variations in chip loads and maximum tool acceleration magnitudes, while maintaining very competitive path traversal times.

The feedrate modulation methodology presented herein can be extended to accommodate other important technical considerations in CNC machining, including variable depths of cut, limits on machine axis acceleration and jerk, minimization of variations in the material removal rate and associated cutting forces, and avoidance of very low or high feedrates to prevent rubbing of the tool against the workpiece and regenerative tool chatter. However, these are non-trivial extensions that deserve separate in-depth investigations.

Publisher's Note Springer Nature remains neutral with regard to jurisdictional claims in published maps and institutional affiliations.

References

1. Altintas Y, Erkorkmaz K (2003) Feedrate optimization for spline interpolation in high speed machine tools. CIRP Ann 52:297–302
2. Cheng M-Y, Su K-H, Wang S-F (2009) Contour error reduction for free-form contour following tasks of biaxial motion control systems. Robot Comput Integ Manuf 25:323–333
3. Chou J-J, Yang DCH (1991) Command generation for three-axis CNC machining. ASME J Eng Indus 113:305–310
4. Conway JR, Ernesto CA, Farouki RT, Zhang M (2012) Performance analysis of cross-coupled controllers for CNC machines based upon precise real-time contour error measurement. Inter J Mach Tools Manuf 52:30–39
5. Dong J, Stori JA (2007) Optimal feed-rate scheduling for high-speed contouring. ASME J Manuf Sci Eng 129:63–76

6. Dong J-C, Wang T-Y, Wang Z-J, Li B, Ding Y-Y, Jiang Y-X (2013) Generalized look-ahead feedrate planning algorithm. Comput Integ Manufac Syst 19:529–539
7. Du D-S, Liu Y-D, Guo X-G, Yamazaki K, Fujishima M (2010) An accurate adaptive NURBS curve interpolator with real-time flexible acceleration/deceleration control. Robot Comput Integ Manuf 26:273–281
8. Elber G, Lee I-K, Kim M-S (1997) Comparing offset curve approximation methods. IEEE Comput Graph Appl 17(3):62–71
9. Erkorkmaz K, Heng M (2008) A heuristic feedrate optimization strategy for NURBS toolpaths. CIRP Ann 57:407–410
10. Erkorkmaz K, Layegh SE, Lazoglum I, Erdim H (2013) Feedrate optimization for freeform milling considering constraints from the feed drive system and process mechanics. CIRP Ann 62:395–398
11. Ernesto CA, Farouki RT (2012) High-speed cornering by CNC machines under prescribed bounds on axis accelerations and toolpath contour error. Int J Adv Manuf Technol 58:327–338
12. Ernesto CA, Farouki RT (2010) Solution of inverse dynamics problems for contour error minimization in CNC machines. Int J Adv Manuf Technol 49:589–604
13. Farouki RT (1994) The conformal map $z \rightarrow z^2$ of the hodograph plane. Comput Aided Geom Des 11:363–390
14. Farouki RT (2008) Pythagorean–Hodograph Curves: Algebra and Geometry Inseparable. Springer, Berlin
15. Farouki RT (2018) Reduced difference polynomials and self-intersection computations. Appl Math Comput 324:174–190
16. Farouki RT, Manjunathaiah J, Nicholas D, Yuan G-F, Jee S (1998) Variable–feedrate CNC interpolators for constant material removal rates along Pythagorean–hodograph curves. Comput Aided Des 30:631–640
17. Farouki RT, Neff CA (1990) Analytic properties of plane offset curves. Comput Aided Geom Des 7:83–99
18. Farouki RT, Neff CA (1990) Algebraic properties of plane offset curves. Comput Aided Geom Des 7:101–127
19. Farouki RT, Shah S (1996) Real-time CNC interpolators for Pythagorean–hodograph curves. Comput Aided Geom Des 13:583–600
20. Farouki RT, Srinathu J (2017) A real-time CNC interpolator algorithm for trimming and filling planar offset curves. Comput Aided Des 86:1–11
21. Farouki RT, Tsai Y-F (2001) Exact Taylor series coefficients for variable-feedrate CNC curve interpolators. Comput Aided Des 33:155–165
22. Hardwick M, Loffredo D (2006) Lessons learned implementing STEP–NC AP–238. Int J Comput Integ Manuf 19:523–532
23. Held M (1991) On the computational geometry of pocket machining. Springer, Berlin
24. Heng M, Erkorkmaz K (2010) Design of a NURBS interpolator with minimal feed fluctuation and continuous feed modulation capability. Inter J Mach Tools Manuf 50:281–293
25. Huang J-T, Yang DCH (1992) A generalized interpolator for command generation of parametric curves in computer-controlled machines. In: Proceedings of Japan/USA Symposium on Flexible Automation, vol 1. ASME, pp 393–399
26. Komanduri R, Subramanian K, Turkovich BF (1984) High speed machining, PED–vol 12. ASME, New York
27. Lee A-C, Lin M-T, Pan Y-R, Lin W-Y (2011) The feedrate scheduling of NURBS interpolator for CNC machine tools. Comput Aided Des 43:612–628
28. Lin K-C, Yang S-Y (2013) Dynamic feedrate control based on the feedback of path curvature and real-time contour error. In: Proceedings, 2013 IEEE 10th International Conference on Power Electronics and Drive Systems (PEDS 2013), pp 370–372
29. Lin R-S, Koren Y (1996) Real-time interpolators for multi-axis CNC machine tools. Manuf Syst 25:145–149
30. Liu H, Liu Q, Yuan S-M (2017) Adaptive feedrate planning on parametric tool path with geometric and kinematic constraints for CNC machining. Int J Adv Manuf Technol 90:1889–1896
31. Nittler KM, Farouki RT (2017) Efficient high-speed cornering motions based on continuously-variable feedrates II.experimental performance analysis. Int J Adv Manuf Technol 88:159–174
32. Pham B (1992) Offset curves and surfaces: a brief survey. Comput Aided Des 24:223–229
33. Ridwan F, Xu X, Liu G-Y (2012) A framework for machining optimization based on STEP-NC. J Intell Manuf 23:423–441
34. Schraeder TF, Farouki RT (2014) Experimental performance analysis of an inverse dynamics CNC compensation scheme for high-speed execution of curved toolpaths. Int J Adv Manuf Technol 73:195–208
35. Smith S, Tlusty J (1997) Current trends in high-speed machining. ASME J Manuf Sci Eng 119:664–666
36. Struik DJ (1961) Lectures on classical differential geometry. Dover Publications (reprint), New York
37. Suh S-H, Cho J-H, Hong H-D (2002) On the architecture of intelligent STEP-compliant CNC. Int J Comput Integ Manuf 15:168–177
38. Sun Y-W, Zhou J-F, Guo D-M (2013) Variable feedrate interpolation of NURBS toolpath with geometric and kinematical constraints for five-axis CNC machining. J Syst Sci Complex 26:757–776
39. Timar SD, Farouki RT, Smith TS, Boyadjieff CL (2005) Algorithms for time-optimal control of CNC machines along curved tool paths. Robot Comput Integ Manuf 21:37–53
40. Tlusty J (1993) High-speed machining. CIRP Ann 42:733–738
41. Yang DCH, Kong T (1994) Parametric interpolator versus linear interpolator for precision CNC machining. Comput Aided Des 26:225–234
42. Wang X, Liu N-F, Wang M-B (2011) Research and implementation of high-precision biaxial tracking control sytem based on NURBS interpolator. Int J Adv Manuf Technol 52:255–262